I&EC research
Industrial & Engineering Chemistry Research

Article

Cite This: Ind. Eng. Chem. Res. 2018, 57, 12916−12925

pubs.acs.org/IECR

Adsorptive Removal of Formaldehyde from Air Using Mixed-Metal Oxides

Anirudh Krishnamurthy, Harshul Thakkar, Ali A. Rownaghi, and Fateme Rezaei*

Department of Chemical and Biochemical Engineering, Missouri University of Science and Technology, 1101 N. State Street, Rolla, Missouri 65409, United States

Supporting Information

ABSTRACT: Volatile organic air pollutants such as aldehyde compounds have been identified as progressively damaging chemicals impacting human health at small albeit dangerous quantities. This study focuses on evaluating the dynamic adsorption of formaldehyde over binary mixed-metal oxides (MMOs) such as ZrO_2/SiO_2 and TiO_2/SiO_2 with different metal ratios. In addition, a metal−organic framework (MOF), namely, MIL-101(Cr), was synthesized and used as a base adsorbent to which the performance of MMOs was compared. The formaldehyde dynamic adsorption capacity of the materials was determined through breakthrough experiments. Our results indicated that zirconia-based materials exhibit a comparatively higher affinity toward formaldehyde than their titania-based counterparts at very dilute concentrations. In particular, ZrO_2/SiO_2 with weight ratio of 25/75 exhibited a dynamic adsorption capacity of 2.9 mmol/g at room temperature using a formaldehyde concentration of 170 ppm_v, which was comparable to that of MIL-101(Cr). Characterization of the materials before and after formaldehyde exposure indicated that formaldehyde was chemically adsorbed on the MMOs. This study highlights the potential of MMOs for efficient abatement of airborne formaldehyde.

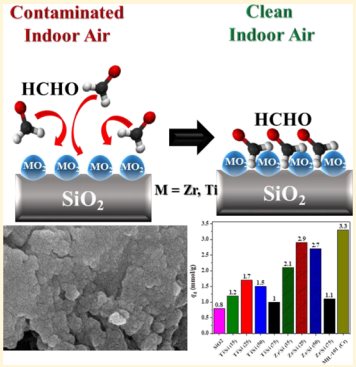

1. INTRODUCTION

As one of the most common types of volatile organic compounds (VOCs), aldehydes are considered as the primary indoor air contaminants. In particular, airborne formaldehyde is among the most toxic VOC compounds in enclosed environments such as commercial or residential buildings. While identifying emissions from individual products may be challenging, the largest sources of formaldehyde in the indoor environment have been identified to be wood floor finishes, wood-based furniture, carpets, and paints.[1−3] The concentration levels are typically dependent upon various factors such as formaldehyde sources, temperature, humidity, and air exchange rate. Catalytic oxidation is a highly efficient approach for abating formaldehyde; however, this method requires the use of expensive noble metals and external thermal energy.[4] The abatement of airborne pollutants in enclosed environments by adsorption has been shown to be the most effective method for air quality control.[5−8] This method is particularly efficient given the dilute concentration of formaldehyde.

To date, various materials such as activated carbons,[2,9−13] amine-modified mesoporous silica,[14−16] metal−organic frameworks (MOFs),[17] mesoporous alumina,[18] layered manganese oxide,[19] boron nitride,[20] transition metal doped graphene,[21] and mixed-metal oxides (MMOs)[22,23] have been investigated for formaldehyde removal from indoor air with activated carbon being the most widely used adsorbent. One of the early studies on the adsorption of formaldehyde was performed by Eriksson et al.[24] on different adsorbents such as activated carbon and alumina in a household environment. Although the experiment showed positive results, the accurate adsorption potential of HCHO was not determined due to its interactions with other pollutants. Due to the polar nature of formaldehyde, the adsorption on activated carbon is not very efficient, and thus surface modifications by primarily nitrogen and amines have been widely practiced to address this issue. Boonamnuayvitaya et al.[9] evaluated a series of activated carbons for formaldehyde adsorption and demonstrated that $ZnCl_2$-impregnated carbon activated with nitrogen shows highest affinity toward formaldehyde due to the hydrophilic functional groups (e.g., O−H, C═O, C−O) on the surface. It was concluded that surface chemistry and physical properties play an important role in formaldehyde abatement. Similar findings were reported by Rong et al.[10,11] In another study, amine functionalization proved to be a facile strategy to significantly improve adsorptive performance of activated carbon in formaldehyde abatement.[13] Passive control of formaldehyde by air-cleaning materials by which formaldehyde gas is decomposed into CO_2 at room temperature has also been reported.[25] The air-cleaning materials consisting of activated carbon particles and manganese oxides reduced formaldehyde concentration from 0.21 to 0.04 ppm_v.

Srisuda and Virote[15] tested amine-modified mesoporous silica for the adsorption of formaldehyde vapor, and results

Received: July 2, 2018
Revised: August 25, 2018
Accepted: August 31, 2018
Published: August 31, 2018

DOI: 10.1021/acs.iecr.8b02962
Ind. Eng. Chem. Res. 2018, 57, 12916−12925

showed a much higher adsorption capacity as compared to activated carbon owing to their amine groups and large pore size of the mesoporous silica support. Moreover, the characterization results confirmed the reaction between formaldehyde molecules and amine groups on pore surface of the adsorbents. In another investigation,[16] the use of amine-functionalized MCM-41 and SBA-15 as adsorbents for formaldehyde vapor from contaminated air was studied and it was concluded that NH_2-MCM-41 is capable of reducing formaldehyde in indoor air by 80%. Furthermore, the performance of amine-functionalized hierarchically hollow SiO_2 microtubes was evaluated for indoor air purification and a maximum formaldehyde adsorption capacity of 20.65 mg/g was reported for these materials.[14] In recent works by Nomura and Jones,[26−28] amine-functionalized silicates were used for formaldehyde abatement. The authors reported an adsorption capacity of 5.7 mmol/g for silica-supported poly(allylamine) amine when formaldehyde gas concentration was kept at 100 ppm_v.[27]

MOF materials have been largely studied as formaldehyde sensors;[29] however, their capability in adsorptive removal of formaldehyde has been rarely explored. In a recent investigation by Wang et al.,[17] the formaldehyde capture of diamine-modified MIL-101 was studied and an adsorption capacity of 5.49 mmol/g was reported for this material using an initial HCHO concentration of 150 ppm_v, whereas the unmodified MIL-101 exhibited a capacity of 3.34 mmol/g. Although functionalization of porous adsorbents with amine moieties contributes to enhanced formaldehyde capture, there is a potential health risk associated with the amines leaching from the adsorbents in enclosed environments, especially for aminopolymers that have weak bonds with the support.

Various MMOs, in particular TiO_2/SiO_2 and TiO_2/ZrO_2, have been commonly evaluated for the capture of aromatic hydrocarbons such as benzene, toluene, and xylene (BTX compounds).[30−35] However, their use as formaldehyde abatement adsorbents has been scarcely discussed. In a study done by Carlos-Cuellar et al.,[36] a range of metal oxides were studied for the adsorption of formaldehyde, among other carbonyl compounds. It was shown that SiO_2 has the lowest uptake when compared to Fe and Al based oxides. Further analysis also showed that a weak hydrogen bonding was responsible for the interaction between the adsorbent and adsorbate. The acidic character of the material was revealed to be an important factor contributing to a higher uptake potential. Typically, in their elemental state, the use of metal oxides for adsorption faces many challenges including low surface area or low adsorption capacity while utilization with other metal oxides or porous materials broadens their potential in adsorption. In a recent investigation by Yu et al.,[23] SiO_2/TiO_2 composite adsorbents with different TiO_2 content were used for the adsorption of formaldehyde and dehumidification and it was shown that the introduction of TiO_2 improved formaldehyde adsorption capacity under typical indoor concentration levels. Xu et al.[22] synthesized a series of hierarchical porous $Ni(OH)_2/SiO_2$ composites with flake-like nanostructure and evaluated their performance in the removal of formaldehyde from air. A maximum adsorption capacity of 8.30 mg/g was obtained for the composites with a better stability than the parent $Ni(OH)_2$ over six adsorption−desorption cycles. The authors attributed the improved performance to the specific framework and synergistic effect between $Ni(OH)_2$ and SiO_2. Most recently, Chen et al.[37] used hierarchical TiO_2 nanospheres functionalized with diethylenetriamine (DETA) for airborne formaldehyde removal at room temperature. The materials exhibited ∼100% removal efficiency with good degree of recyclability when exposed to 200 ppm_v of formaldehyde.

As noted above, although formaldehyde abatement by adsorption has been the subject of several studies, the majority of the materials investigated so far suffer from low adsorption capacity. Furthermore, the removal of formaldehyde from indoor air has not been investigated over MMO materials that have been shown efficient in capturing other VOCs. In this investigation, we synthesized two different types of MMOs, TiO_2/SiO_2 and ZrO_2/SiO_2, with varying metal oxide ratios and evaluated their formaldehyde adsorption characteristics by performing dynamic breakthrough experiments in a fixed-bed system. In addition, the performance of MIL-10(Cr), as a base adsorbent that has been proven efficient in abating formaldehyde,[17] was evaluated and compared with that of MMOs. The adsorbents were systematically characterized, and their textural and physical properties were correlated with their adsorption performance in abating airborne formaldehyde.

2. EXPERIMENTAL SECTION

2.1. Materials. Tetraethyl orthosilicate (TEOS, 99%), zirconium(IV) propoxide solution (70% in 1-propanol), titanium(IV) butoxide (TBT, reagent grade, 97%), hexadecyltrimethylammonium bromide (CTAB), triethanolamine (TEAH), formaldehyde solution (ACS reagent, 37% in H_2O), chromium nitrate nonahydrate ($Cr(NO_3)_3{\cdot}9H_2O$), terephthalic acid (H_2BDC), and nitric acid (HNO_3) were all purchased from Sigma-Aldrich. Moreover, all solvents were of analytical grade and purchased from Sigma-Aldrich. Ultrahigh purity nitrogen gas was purchased from Airgas.

2.2. Adsorbents Synthesis. *Preparation of Mixed-Metal Oxides.* Binary metal oxides were prepared according to the modified atrane synthesis route described by Ortiz De Zarate et al.[38] Briefly, TEOS was added dropwise to 17.7 mL of TEAH. The required amount of metal alkoxide was added dropwise to the above solution and subsequently heated to 150 °C to obtain atrane complexes. The solution was then cooled to 90 °C followed by the addition of CTAB to the solution. The mixture was then cooled to 60 °C, and 75 mL of DI water was added, and the obtained white colored liquid was set to gel for 24 h at room temperature. The samples were then washed with DI water and ethanol multiple times before drying at 80 °C overnight. The obtained white powders were then calcined at 550 °C for 6 h. The samples obtained were denoted as Ti/Si (x) and Zr/Si (x), where x is the Ti/Zr loading.

Preparation of MIL-101(Cr). The synthesis method followed was a slightly modified procedure used by Zhao et al.[39] Briefly, about 800 mg of chromium nitrate nonahydrate ($Cr(NO_3)_3{\cdot}9H_2O$) and 328 mg of H_2BDC were mixed together and subsequently 180 mg of HNO_3 was added to the mixture. The reactants were mixed and sonicated until a fairly homogeneous solution was obtained. The contents were then transferred to an autoclave and kept at 220 °C for 8 h. The material was then cooled, filtered, and solvent-exchanged. The obtained solid was washed with DMF and DI water and then refluxed in hot ethanol at 70 °C for 5 h.

2.3. Adsorbents Characterization. Low-angle powder X-ray diffraction (XRD) was performed using a PANanalytical X'Pert multipurpose X-ray diffractometer. Diffraction patterns were recorded for all prepared samples to identify their crystal

DOI: 10.1021/acs.iecr.8b02962
Ind. Eng. Chem. Res. 2018, 57, 12916−12925

structure. By use of crystal structure file obtained from the open crystal database, a simulated pattern for MIL-101(Cr) was generated and compared with the synthesized material. Scanning electron microscopy (SEM) was used to assess structural morphology of the materials. This was performed using a Hitachi model S4700 field-emission SEM instrument. N_2 physisorption isotherms were obtained using a Micromeritics 3Flex gas analyzer at 77 K. Degassing in a Micromeritics Prevac was performed for various temperatures at elongated time frames, depending on the material. Surface area was consequently determined using Brunauer–Emmett–Teller (BET), while pore volume was estimated at $P/P_0 = 0.9$. The nonlocal density functional theory (NLDFT) method was also used to determine pore size distribution (PSD) profiles. X-ray photoelectron spectroscopy (XPS) was performed using Kratos Axis 165 photoelectron spectrometer using an aluminum X-ray source to excite the samples. Fourier transform infrared (FTIR) analysis was employed to characterize the chemical structure of the MMOs before and after HCHO adsorption on a Nicolet FTIR model 750 spectrometer.

2.4. Formaldehyde Breakthrough Experiments. Dynamic adsorption capacities of the synthesized materials were measured by performing breakthrough experiments in a lab-scale setup consisting of a borosilicate packed column with the dimensions of 2.5 cm × 20 cm and a mass spectrometer (BELMass), as depicted in Figure 1. About 300 mg of the adsorbent was loaded into the bed and degassed at 130 °C under nitrogen with the flow rate of 40 mL/min prior to test.

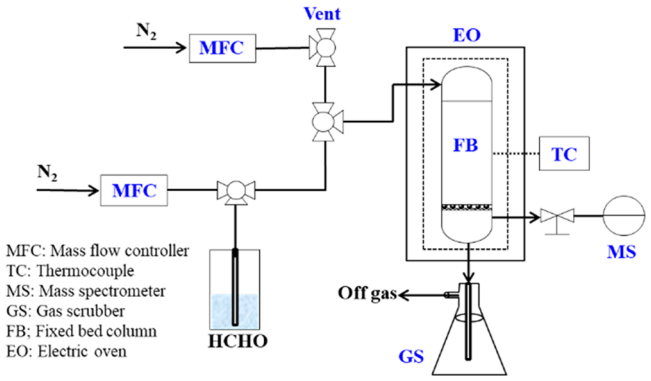

Figure 1. General scheme of the breakthrough setup used for HCHO adsorption tests.

For breakthrough measurements, first formaldehyde solution (37%) was filled into a saturator and a pure N_2 stream at a flow rate of 40 mL/min was used to carry an HCHO vapor concentration of ~170 ppm_v to the column. Experiments were performed at 25 °C and atmospheric pressure. It should be noted here that this concentration is much higher than the realistic formaldehyde levels at an indoor environment (<5 ppm_v); however, to accurately quantify the uptake capacities of the materials, the experiments were conducted under these conditions.

3. RESULTS AND DISCUSSION

3.1. Adsorbents Characterization. The low-angle XRD patterns for all adsorbents are presented in Figure 2. Low-angle XRD was considered in this study due to the nature of the adsorbent particles, which showed low-angle diffraction patterns, typical of interplanar spacing in mesoporous materials.[40] The nanosized particles did not display any diffraction peaks over the angular range of 10–50°. For bare silica, a low-intense peak was observed at $2\theta = 2.5°$ which could be associated with the (100) reflection. For both sets of MMOs, the obtained patterns were characteristic of interparticular short-range hexagonal ordered mesoporous materials, similar to the case of MCM-41.[41] In both cases, the characteristic peaks of 15 and 25 samples were clearly visible but for high loading samples (50 and 75), they were less intense and thus not visible after compiling the spectra (the corresponding XRD spectra for high loading samples are presented in Figure S1, Supporting Information). It is also noted from Figure 2a and Figure 2b that the peak intensity decreased with Ti and Zr loadings indicating that the degree of crystallinity of the silica was lowered by incorporating more Ti/Zr atoms into the mesoporous silica walls. Ortiz De Zarate et al.[38] reported the same decreasing trend in the degree of orderness for their Si/Zr samples.

The XRD diffraction pattern of MIL-101(Cr) was also obtained and compared with a simulated pattern for MIL-101(Cr) obtained from the crystallographic open database in project mercury. As evident from Figure S2, Supporting Information, the XRD profile of the MIL-101(Cr) synthesized in this work corresponded well with the simulated pattern, thereby confirming the successful synthesis of this adsorbent.

N_2 physisorption isotherms obtained at 77 K along with PSD profiles are displayed in Figure 3. As evident from this figure, all MMOs showed a combination of types II and IV isotherms with a H4 hysteresis indicative of their mesopo-

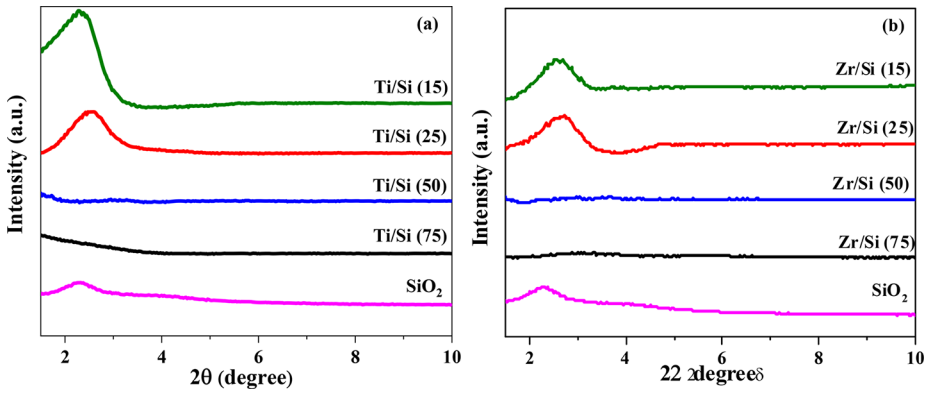

Figure 2. XRD patterns for (a) Ti/Si and (b) Zr/Si adsorbents.

DOI: 10.1021/acs.iecr.8b02962
Ind. Eng. Chem. Res. 2018, 57, 12916–12925

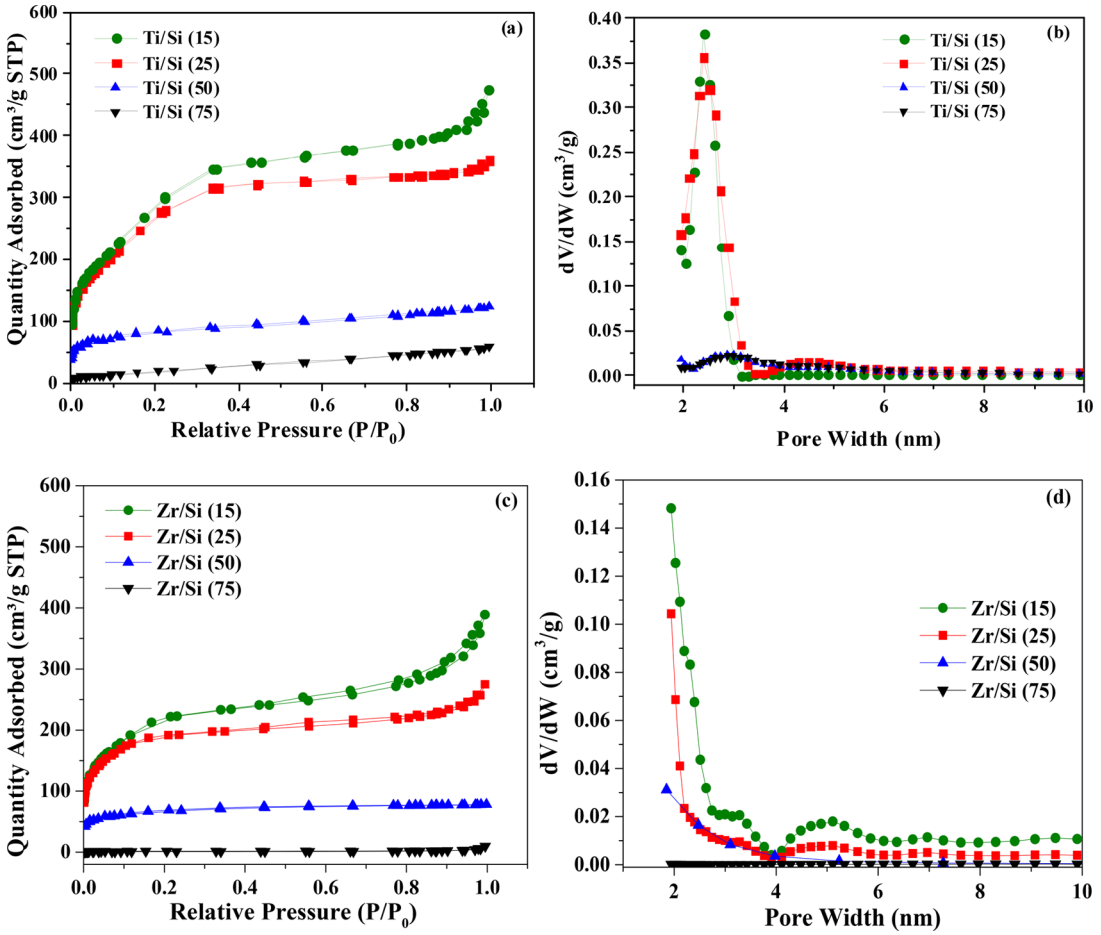

Figure 3. N_2 physisorption isotherms and PSD profiles for (a, b) Ti/Si and (c, d) Zr/Si materials.

rous−macroporous nature. As shown in Figure 3a, increasing Ti loading from 15 to 75 wt % gave rise to dramatic reduction in nitrogen uptake. Moreover, the pore size distribution of titania-doped silica samples ranged from 2 to 5 nm, as shown in Figure 3b. For zirconia-doped silica samples, a similar decreasing trend with Zr content was observed (Figure 3c) with Zr/Si (75) showing essentially zero uptake indicative of its nonporous structure. The PSD profiles displayed in Figure 3d revealed an increase in the average pore size from 2.3 to 3.1 nm for zirconia-doped silica adsorbents. The bare silica showed two distinct adsorption/desorption steps, as demonstrated in Figure S3s, Supporting Information. The first step at lower P/P_0 corresponded to the filling of mesopores.[42] This process seemed to be gradual, unlike the second step at higher P/P_0 which indicated rapid filling of large mesopores and possibly macropores, implying large concentration of uniform mesopores, which can be confirmed in the PSD curve shown in Figure S3b. For MIL-101(Cr) sample, a typical type I isotherm indicative of microporous nature of this MOF was observed (Figure S3c) with uniform pores having sizes on the order of 1.9 nm, as can be observed in Figure S3d.

Textural properties of the adsorbents determined from N_2 physisorption isotherms are quantitatively presented in Table 1. Overall, the BET surface area and pore volume of the MMO samples were lower than those of bare silica material. This was expected as the doped oxides occupy the interparticular, ordered, mesoporous silica during doping process, thus contributing to lower pore volume and surface area. For instance, Ti/Si (15) and Zr/Si (15) exhibited surface areas of 1115 and 768 m^2/g, respectively, compared to 1483 m^2/g surface area of the bare silica. Similarly, they exhibited pore volumes of 0.64 and 0.56 cm^3/g, respectively, while the bare silica displayed a pore volume of 1.35 cm^3/g. A large mesopore volume can be attributed to the ordered and fairly regular sized mesopores obtained due to the incorporation of surfactant molecules within the matrix. This also corresponded to the hexagonal mesophases, commonly detected in such materials,[41] which was also confirmed by XRD results, presented earlier.

Although the textural properties of lower loaded samples (15 and 25) were found to be comparable to those of the bare support, a dramatic loss in surface area and porosity was

Table 1. Textural Properties of the MMOs, Bare Silica, and MIL-101(Cr) Adsorbents

sample	S_{BET} (m^2/g)	V (cm^3/g)	d_p (nm)
bare silica	1483	1.35	3.3
Ti/Si (15)	1115	0.64	2.8
Ti/Si (25)	1030	0.60	2.7
Ti/Si (50)	271	0.18	2.7
Ti/Si (75)	73	0.08	3.1
Zr/Si (15)	768	0.56	2.3
Zr/Si (25)	635	0.40	2.5
Zr/Si (50)	226	0.18	2.3
Zr/Si (75)	4	0.01	3.1
MIL-101(Cr)	2200	1.16	1.9

DOI: 10.1021/acs.iecr.8b02962
Ind. Eng. Chem. Res. 2018, 57, 12916−12925

noticed with increasing metal content to 50 and 75 wt %. The BET surface area dropped to 73 and 4 m^2/g, and pore volume decreased to 0.08 and 0.01 cm^3/g for Ti/Si (75) and Zr/Si (75), respectively. Another observable trend was the comparatively better surface properties of Ti/Si (x) when compared to Zr/Si (x) which stemmed from the larger size of ZrO_2 nanoparticles with a greater portion of the surface being occupied when compared to its TiO_2 counterpart. MIL-101(Cr) was shown to have superior surface characteristics when compared to the metal oxide samples, as expected, with a BET surface area of 2200 m^2/g and a pore volume of 1.16 cm^3/g.

Figure 4 illustrates the SEM images of MMOs with low (15) and high (75) metal loadings. High- and low-level magnification images were obtained to compare the surface morphology of different adsorbents. What can be observed from Figure 4a,b is spherical nanoparticles similar to that of UVM-7 silica[42] for Ti/Si (15), whereas for highly loaded sample, Ti/Si (75), the particles sintering and agglomeration were observed (Figure 4c,d). A relatively similar morphology was obtained for Zr-based samples, with lower-doped adsorbent having a more pronounced spherical particle shape (Figure 4e,f), as opposed to the higher-doped sample which exhibited a high degree of particles agglomeration and irregular particle shapes, as seen in Figure 4g,h. Such high degree of agglomeration may explain the dramatic decrease in pore volume of both highly loaded titania and zirconia MMOs, as shown in Table 1. Comparison of the higher-doped Ti/Si and Zr/Si materials revealed that the degree of agglomeration and sintering was much higher for Zr/Si (75) than for Ti/Si (75) which can explain the large difference in their surface characteristics. Notably, almost all adsorbents showed some macropores in the range 60−100 nm. Considering the microporous MIL-101(Cr), Figure S4a,b confirms the formation of well-intergrown crystals with octahedron shape and sizes in the range of 20−300 nm, as expected.

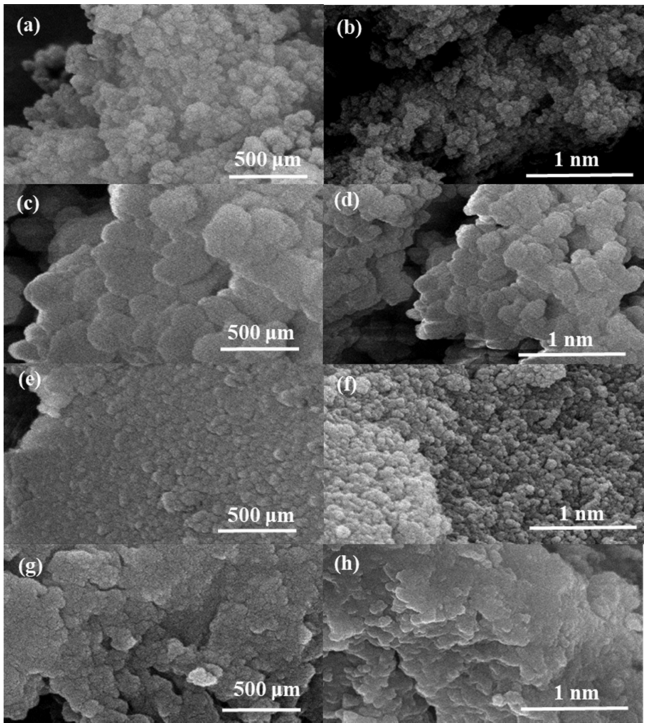

Figure 4. High- and low-magnification SEM images of (a, b) Ti/Si (15), (c, d) Ti/Si (75), (e, f) Zr/Si (15), and (g, h) Zr/Si (75).

Figure 5 illustrates the XPS spectra obtained for the MMO samples. From Figure 5a and Figure 5c, two distinct Si peaks were detected at 103 and 154 eV which correspond to SiO_2 in the 2p and 2s atomic levels, respectively. The presence of these peaks confirmed the existence of SiO_2 groups within the MMO materials prepared. The most prominent oxygen peak, which was detected in all samples at 530 eV, corresponded to oxygen in the 1s atomic level. This peak also had the highest intensity, which can be seen in the results derived from XPS, listed in Table 2 and is the atomic level of oxygen present in metal oxides in general. What was also noticeable was the decrease in intensity of the peaks as the Ti or Zr content increased. Shown in Figure 5b are the Ti spectra obtained for Ti/Si samples. Ti/Si (15) and Ti/Si (25) showed a lack of Ti 3s and 3p atomic levels which could be correlated to the smaller content of TiO_2 in these samples. All samples, however, showed a spin orbital splitting at Ti 2p and Ti $2p_{1/2}$ atomic levels. This corresponded to the atomic levels commonly detected in TiO_2 which further confirmed the formation of TiO_2 on the SiO_2 support. With the increase in TiO_2 content, the expected reduction in peak intensities was detected. In the case of Zr/Si materials (Figure 5d), a larger number of atomic levels were detected, possibly implying a larger degree of bonding between the two metal oxides when compared to Ti/Si materials. Notably, the Zr 4s and 4p atomic levels were not detected in Zr/Si (15) and (25) samples, whereas, the Zr 3s, 3p, and 3d levels were observed in all samples, with decreasing intensities with ZrO_2 content. Figure S4, Supporting Information, depicts the results obtained for the bare silica. There were no peaks detected in the Ti and Zr range; however, the Si and O peaks were found to be similar to those of MMO samples with lowest loadings.

Table 2 illustrates the atomic concentrations calculated from the XPS results. The concentrations were calculated using Si 2p, O 1s, Ti 2p, and Zr 3d. Silica atomic levels were found to be quantitatively fairly constant, while the amount of doped metal oxide was changed. Metal loading was calculated by the metal to Si ratio. The estimated titania loadings actually achieved were found to be slightly different from target loadings with no particular trend observed with the Si or O concentrations. The actual zirconia concentration was found to be lower than expected which could be attributed to the leaching process during the sol−gel preparation method. Si content was also found to decrease with an increase in zirconia loading. Notably, Zr/Si (25) was found to have a fairly large O concentration (49%), which could also be in reference to the large hydroxyl groups concentration within the adsorbent matrix. It should be pointed out here that C 1s was also detected in the spectra due to the carbon tape used in the measurement.

3.2. Dynamic Adsorption Performance. Fixed-bed adsorption experiments were performed to determine dynamic adsorption capacity of the adsorbent materials. Formaldehyde vapor concentration in the inlet gas stream was calculated to be ~170 ppm_v at room temperature and atmospheric pressure. Moreover, we used eq 1 to estimate the amount of formaldehyde adsorbed onto the adsorbents,

$$q_d = \frac{Q_F C_0 t_s}{W} \quad (1)$$

where Q_F is the inlet feed flow rate, C_0, formaldehyde feed concentration, W is the weight of the adsorbent, and t_s is the

DOI: 10.1021/acs.iecr.8b02962
Ind. Eng. Chem. Res. 2018, 57, 12916−12925

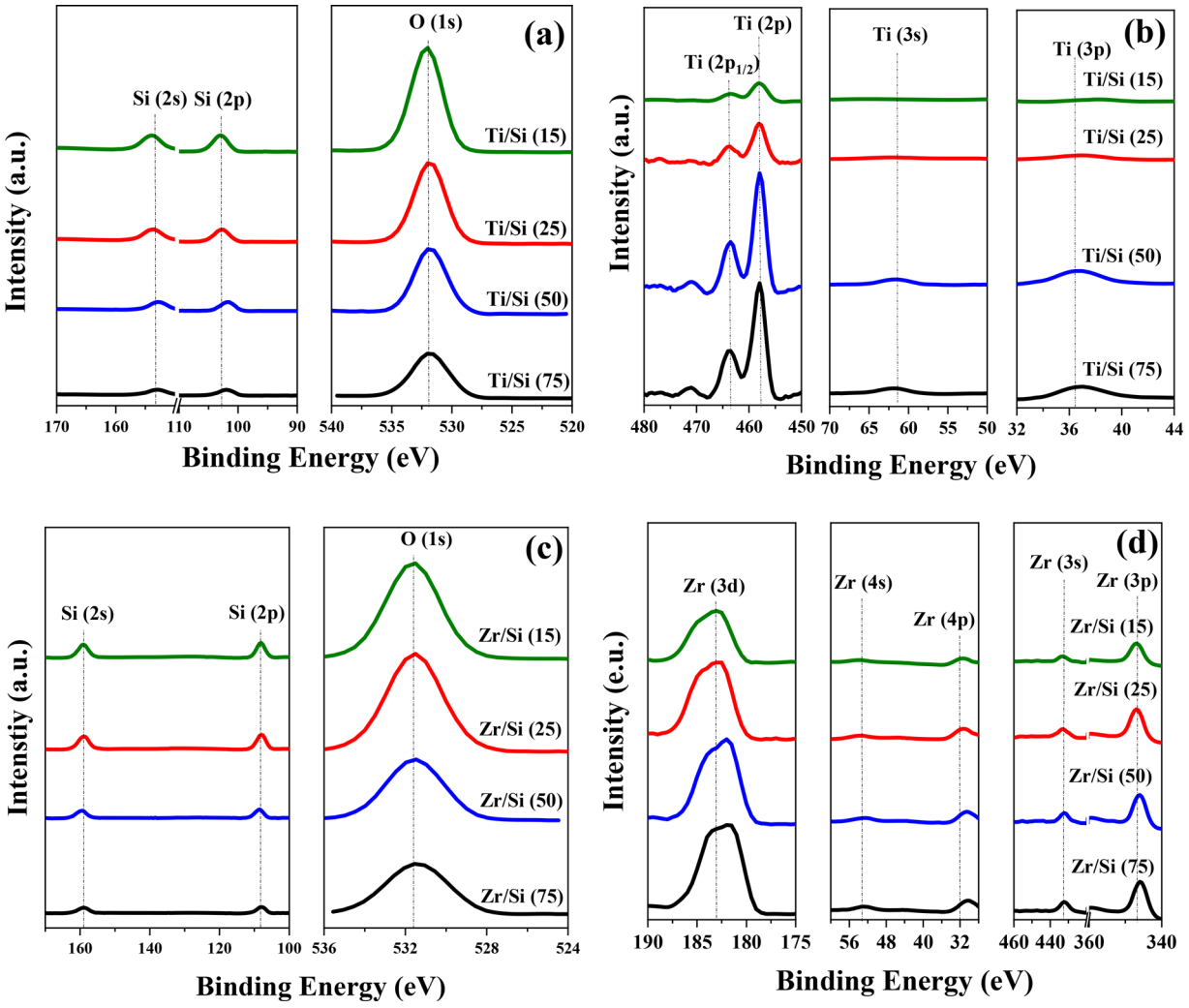

Figure 5. XPS spectra for MMO samples: (a) Si and O spectra for Ti/Si, (b) Ti spectra for Ti/Si, (c) Si and O spectra for Zr/Si, and (d) Zr spectra for Zr/Si materials.

Table 2. Elemental Composition and the Metal Loading of the MMOs Determined by XPS

sample	Ti or Zr (atom %)	Si (atom %)	O (atom %)	Ti or Zr loading (wt %)
Ti/Si (15)	2	24	66	8
Ti/Si (25)	5	34	56	15
Ti/Si (50)	13	24	45	54
Ti/Si (75)	19	23	49	82
Zr/Si (15)	3	23	51	13
Zr/Si (25)	5	22	49	22
Zr/Si (50)	7	17	41	43
Zr/Si (75)	10	16	40	62

stoichiometric time, which can be estimated from the breakthrough profile using eq 2,

$$t_s = \int_0^\infty \left(1 - \frac{C}{C_0}\right) \partial t \tag{2}$$

In the above equation, C is the formaldehyde concentration at the column outlet at time t.

Figure 6 illustrates the formaldehyde breakthrough profiles over the adsorbents investigated, while Figure 7 and Table 3 show the comparison of the corresponding dynamic capacities (q_d) estimated from eq 1. Overall, the formaldehyde adsorption on MIL-101(Cr) was higher than on the MMOs, as characterized by a longer breakthrough time with an uptake capacity of 3.3 mmol/g. The capacity obtained for MIL-101(Cr) was comparable with the literature data reported before.[43] What was immediately noticeable was that the incorporation of the second metal oxide led to an enhancement of adsorption capacity of formaldehyde in comparison to the bare silica. For the family of Ti/Si samples, 25 wt % titania supported on silica was found to have the highest capacity at q_d = 1.7 mmol/g, whereas the other samples were in a slightly lower range (approximately 1.1−1.2 mmol/g). It was also found that increasing the Ti content from 0 to 25 wt % led to improved capture capacity but with further increase to 75 wt %, an opposite trend resulted (see Figure 6a). This behavior could be explained by the fact that the amount of doped titania increases the amount of surface hydroxyl groups, which have been previously identified to be the main active sites for adsorption of formaldehyde over metal oxides by forming hydrogen bonds with formaldehyde molecules.[44,45] Through in situ DRIFTS and step scanning XRD measurements, Wang et al.[19] showed that formaldehyde adsorption over layered manganese oxide is promoted by bonded water via hydrogen bonding. It is also important to note that adsorption kinetics

DOI: 10.1021/acs.iecr.8b02962
Ind. Eng. Chem. Res. 2018, 57, 12916−12925

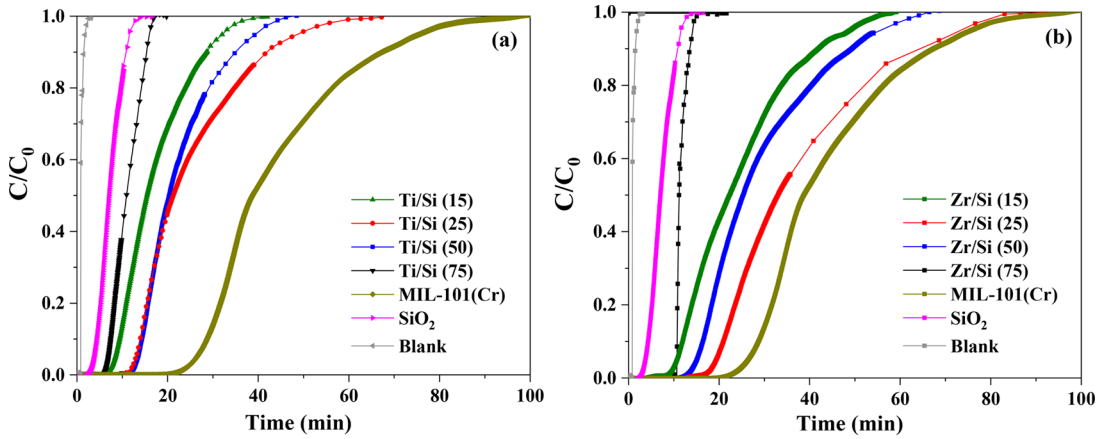

Figure 6. Formaldehyde breakthrough profiles over (a) Ti/Si and (b) Zr/Si adsorbents with comparison with Mil-101(Cr) profile.

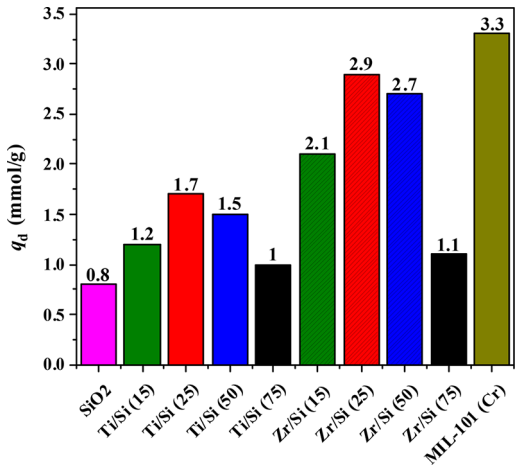

Figure 7. Dynamic adsorption capacity of formaldehyde estimated from breakthrough profiles obtained at room temperature and atmospheric pressure using 170 ppm_v of formaldehyde vapor.

Table 3. Comparison of Stoichiometric Time and Dynamic Adsorption Capacity of Formaldehyde for All Adsorbents

sample	t_s (min)	q_d (mmol/g)
bare silica	12	0.8
Ti/Si (15)	40	1.2
Ti/Si (25)	55	1.7
Ti/Si (50)	43	1.5
Ti/Si (75)	17	1.0
Zr/Si (15)	56	2.1
Zr/Si (25)	72	2.9
Zr/Si (50)	62	2.7
Zr/Si (75)	39	1.1
MIL-101(Cr)	90	3.3

were shown to be slightly slower in the case of Ti/Si (25) when compared to other materials in its family, indicated by a long tail, which may limit the use of this material for cyclic operations. As the loading of titania increased, the semi-equilibrium capacities decreased which could be attributed to the decrease in surface area and pore volume with metal loading.

In the case of zirconia samples, a similar trend was observed in which the highest semiequilibrium capacity was displayed by Zr/Si (25) at q_d = 2.9 mmol/g, which was close to that of MIL-101(Cr). However, upon increasing the ZrO_2 loading from 25 to 50 wt %, a slight drop in capacity (q_d = 2.9−2.7 mmol g^{-1}) was observed. Although increasing the loading from 15 to 25 wt %, showed a 45% enhancement in formaldehyde adsorption, an opposite trend was observed for higher loadings and the capacity dropped by ∼45% for Zr/Si (75). Furthermore, investigating the breakthrough profiles in Figure 6b revealed that unlike titania-based adsorbents, diffusional resistances became more pronounced for zirconia-based samples resulting in relatively broad profiles, which could be attributed to the large degree of agglomeration for ZrO_2 particles, as observed by SEM images, which limited the accessibility and diffusion of the adsorbate molecules to the adsorption sites in the pores of the adsorbent. The higher capacities obtained from the Zr/Si (x) samples compared to the Ti samples can be explained by surface acidity. It has been proven that Zr/Si materials show a higher acidity than Ti/Si materials, which could be an influential factor in the uptake values recorded in this investigation.[46] Furthermore, the level of hydroxyl bonding in case of zirconia materials has been shown to be much higher[44] than their titania counterparts. As a control experiment, bare silica (SiO_2) was also tested for HCHO adsorption, as evident from Figures 6 and 7. Despite very high surface characteristics, it showed the lowest semi-equilibrium capacity at 0.8 mmol/g when compared to all the MMO samples, owing to the poor interaction of formaldehyde molecules with its surface. Overall, these results indicated that Zr/Si adsorbents have a higher affinity toward HCHO when compared to Ti/Si adsorbents for the airborne abatement of formaldehyde and that the incorporation of titania and zirconia into the mesoporous silica promotes the formaldehyde uptake of silica. Considering the low costs to prepare this material and its comparable performance to MIL-101(Cr), a MOF commonly used for VOC abatement that is expensive to synthesize, zirconia-based materials could potentially be promising candidates for abating formaldehyde and other VOCs.

To determine the presence of hydroxyl groups in MMOs, FTIR analysis was employed and the corresponding FTIR spectra are illustrated in Figure 8. For all materials, a band detected between 998 and 1234 cm^{-1} corresponded to the fundamental component of these materials. This range depicted the SiO_4 and Si−O−Si absorption bands and was indicative of the role of silica in these materials as a support and as a building block for these MMO materials.[47] An

DOI: 10.1021/acs.iecr.8b02962
Ind. Eng. Chem. Res. 2018, 57, 12916−12925

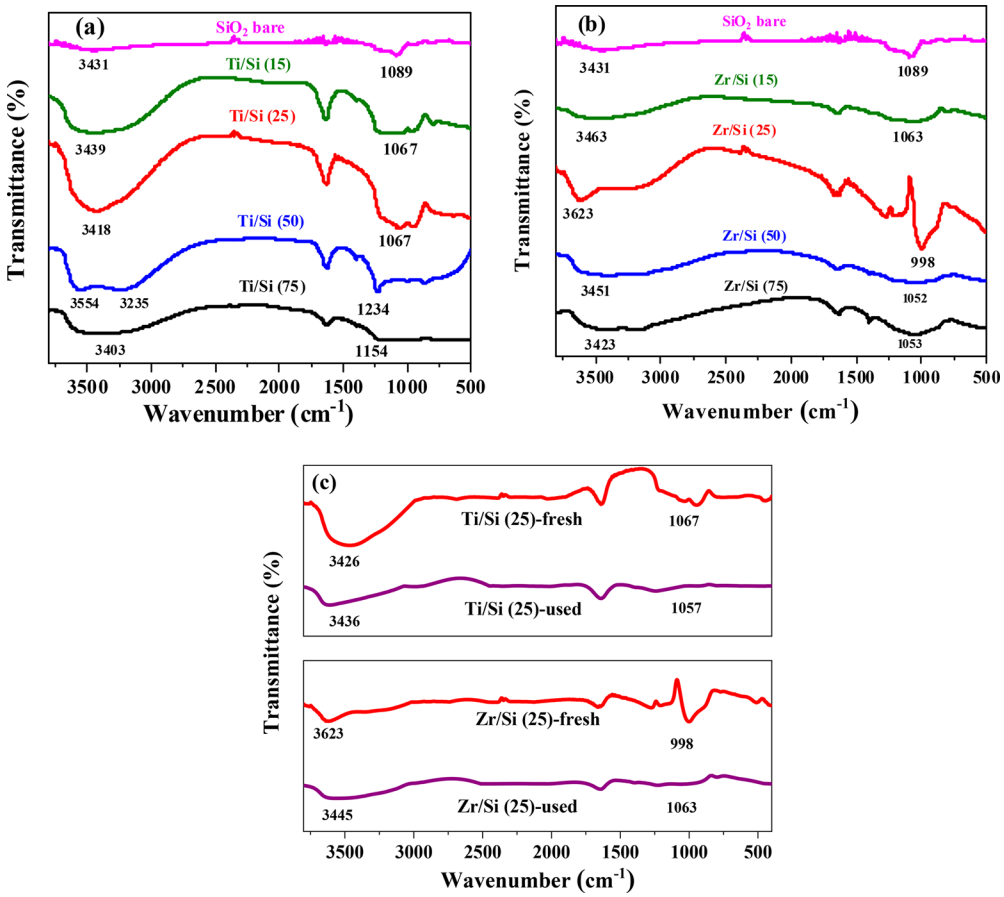

Figure 8. (a) FTIR spectra obtained for (a) Ti/Si, (b) Zr/Si adsorbents along with the bare silica, and (c) fresh and used samples.

absorption band observed at around 920 cm^{-1} for both classes of MMO samples correlated to Si−O−M bond,[48,49] where M = Si/Ti. The broad peaks beyond 3000 cm^{-1} were assigned to O−H stretching vibrations. These bands depict the hydroxyl groups that are present in the materials. From Figure 8a, in the case of the titania samples, multiple smaller peaks were also observed in the 500−700 cm^{-1} range for titania samples, suggesting that titania was present in its anatase phase within the MMO system.[50] Higher loadings of titania displayed a shift in SiO_4 vibration modes, suggesting that the loading of titania affected the primary silica structure. Peaks around 1639 cm^{-1} referred to the bending modes of H−O−H, which was an indication of chemisorbed water on the surface of the materials.[51] Peaks in the range of 3235−3554 cm^{-1} represented the surface hydroxyl groups present in the samples. Ti/Si (25) showed the largest concentration of surface hydroxyl groups quantitatively, which fell in line with semiequilibrium adsorption measurements. As the titania loading increased, a drop in the number of hydroxyl groups was observed for these samples. Figure 8b illustrates the spectra obtained for zirconia samples. Peaks between 998 and 1063 cm^{-1} were assigned to asymmetric stretching of the SiO_4 unit.[48] Peaks observed in the zirconia samples displayed a more similar absorption band when compared to bare SiO_2, indicating that the silica network was fairly maintained for the zirconia sample. This also highlights the fact that each Zr atom was coordinated with the SiO_4 molecule through an edge and corner connection.[52] The peak obtained around 1050−1063 cm^{-1} indicated the presence of SiO_4^- tetrahedra. In contrast to their titania counterparts, zirconia samples showed either very minimal or no peaks at the 1640 cm^{-1} range, which suggested the effect of humidity could potentially be insignificant. As observed with titania samples, the number of surface hydroxyl groups reached a maximum for the 25/75 loading, proving our hypothesis that the hydroxyl groups were indeed responsible for improved HCHO adsorption. Comparing the FTIR spectra of the MMO samples in both figures revealed that while hydroxyl group peaks were observed for the titania samples as well, they were less intense compared to zirconia samples. This could also be the reason for zirconia's superior adsorption characteristics over titania samples.

Figure 8c compares the FTIR spectra obtained for fresh and used Ti/Si (25) and Zr/Si (25) samples that exhibited the largest HCHO uptake among their family. The range of peaks below 1200 cm^{-1} seemed to be less evident in the used samples, suggesting the slight deformation of the MMO matrix due to the adsorption of formate ions on the surface hydroxyl groups. Furthermore, the different types of charged ions being adsorbed onto the surface could have caused structural changes, as shown previously.[45] Comparison of the FTIR spectra of fresh and used adsorbents revealed that the adsorbed HCHO affected the structure of the adsorbents for both samples. Notably, beyond 3000 cm^{-1}, a shift in the hydroxyl group peaks was observed, which depicted the reduction in the number of available surface hydroxyl groups after adsorption. Wang et al.[19] showed that both bonded water and water in the air can stimulate the desorption of formate formed on the metal oxide surface as a result of formaldehyde adsorption at room temperature, thereby recovering the adsorption capacity and regenerating the materials.

DOI: 10.1021/acs.iecr.8b02962
Ind. Eng. Chem. Res. 2018, 57, 12916−12925

4. CONCLUSIONS

This paper provides insight into the formaldehyde removal from indoor air using mixed-metal oxide adsorbents. A series of titania- and zirconia-doped silica materials were synthesized, and their formaldehyde adsorption performance was investigated by dynamic breakthrough experiments. In addition, MIL-101(Cr) was synthesized and used as a base adsorbent for comparing the adsorptive characteristics of MMOs. The obtained capacities were correlated with the titania/zirconia loading, and it was demonstrated that zirconia samples are more efficient in abating airborne formaldehyde than their titania analogues. A maximum dynamic capacity of 2.9 mmol/g was observed for Zr/Si (25) which was comparable to that of MIL-101(Cr) with a capacity of 3.3 mmol/g when exposed to 170 ppm_v formaldehyde vapor. Furthermore, the characterization of the materials after experiments highlighted chemisorption of formaldehyde on the surface of MMOs which could be desorbed upon exposure to water in air. The findings reported in this investigation reveal the potential of titania- and zirconia-based mixed-metal oxides as efficient solid adsorbents in the abatement of formaldehyde vapor.

■ ASSOCIATED CONTENT

Supporting Information

The Supporting Information is available free of charge on the ACS Publications website at DOI: 10.1021/acs.iecr.8b02962.

XRD patterns, N_2 physisorption isotherms and pore size distributions, SEM images, and XPS spectra (PDF)

■ AUTHOR INFORMATION

Corresponding Author

*E-mail: rezaeif@mst.edu.

ORCID

Ali A. Rownaghi: 0000-0001-5228-5624

Fateme Rezaei: 0000-0002-4214-4235

Notes

The authors declare no competing financial interest.

■ ACKNOWLEDGMENTS

This work was supported by the National Science Foundation (NSF Grant CBET-1802049). The authors also thank Materials Research Center (MRC) of Missouri S&T for SEM and XRD measurements.

■ NOMENCLATURE

C = formaldehyde concentration at the column outlet at time t, mmol mL^{-1}

C_0 = formaldehyde feed concentration, mmol mL^{-1}

d_p = average pore size, nm

q_d = amount of formaldehyde adsorbed onto the adsorbent, mmol g^{-1}

Q_F = inlet feed flow rate, mL min^{-1}

S_{BET} = BET surface area, m^2 g^{-1}

t = adsorption time, min

t_s = stoichiometric time, min

V = pore volume, cm^3 g^{-1}

W = weight of the adsorbent, g

■ REFERENCES

(1) Callahan, C. M. *An Update on Formaldehyde*; U.S. Consumer Product Safety Commission: Bethesda, MD, 2016.

(2) Carter, E. M.; Katz, L. E.; Speitel, G. E.; Ramirez, D. Gas-Phase Formaldehyde Adsorption Isotherm Studies on Activated Carbon: Correlations of Adsorption Capacity to Surface Functional Group Density. *Environ. Sci. Technol.* **2011**, *45* (15), 6498.

(3) Zhang, X.; Gao, B.; Creamer, A. E.; Cao, C.; Li, Y. Adsorption of VOCs onto Engineered Carbon Materials: A Review. *J. Hazard. Mater.* **2017**, *338*, 102.

(4) Torres, J. Q.; Royer, S.; Bellat, J. P.; Giraudon, J. M.; Lamonier, J. F. Formaldehyde: Catalytic Oxidation as a Promising Soft Way of Elimination. *ChemSusChem* **2013**, *6* (4), 578.

(5) Khan, N. A.; Hasan, Z.; Jhung, S. H. Adsorptive Removal of Hazardous Materials Using Metal-Organic Frameworks (MOFs): A Review. *J. Hazard. Mater.* **2013**, *244*−*245*, 444.

(6) Rajan, P. E.; Krishnamurthy, A.; Morrison, G.; Rezaei, F. Advanced Buffer Materials for Indoor Air CO_2 Control in Commercial Buildings. *Indoor Air* **2017**, *27*, 1213.

(7) Green, G. D.; Swedo, R. J.; Tomlinson, I. A.; Whetten, A. R.; Coburn, C. E.; Henning, M. A.; Novy, P. M. Methods for Reducing Airborne Formaldehyde. Patent 8236263 B2, 2012.

(8) Sidheswaran, M. A.; Destaillats, H.; Sullivan, D. P.; Cohn, S.; Fisk, W. J. Energy Efficient Indoor VOC Air Cleaning with Activated Carbon Fiber (ACF) Filters. *Build. Environ.* **2012**, *47* (1), 357.

(9) Boonamnuayvitaya, V.; Sae-ung, S.; Tanthapanichakoon, W. Preparation of Activated Carbons from Coffee Residue for the Adsorption of Formaldehyde. *Sep. Purif. Technol.* **2005**, *42* (2), 159.

(10) Rong, H.; Ryu, Z.; Zheng, J.; Zhang, Y. Effect of Air Oxidation of Rayon-Based Activated Carbon Fibers on the Adsorption Behavior for Formaldehyde. *Carbon* **2002**, *40*, 2291.

(11) Li, J.; Li, Z.; Liu, B.; Xia, Q.; Xi, H. Effect of Relative Humidity on Adsorption of Formaldehyde on Modified Activated Carbons. *Chin. J. Chem. Eng.* **2008**, *16* (6), 871.

(12) Das, D.; Gaur, V.; Verma, N. Removal of Volatile Organic Compound by Activated Carbon Fiber. *Carbon* **2004**, *42* (14), 2949.

(13) Ma, C.; Li, X.; Zhu, T. Removal of Low-Concentration Formaldehyde in Air by Adsorption on Activated Carbon Modified by Hexamethylene Diamine. *Carbon* **2011**, *49* (8), 2873.

(14) Le, Y.; Guo, D.; Cheng, B.; Yu, J. Bio-Template-Assisted Synthesis of Hierarchically Hollow SiO_2 Microtubes and Their Enhanced Formaldehyde Adsorption Performance. *Appl. Surf. Sci.* **2013**, *274*, 110.

(15) Srisuda, S.; Virote, B. Adsorption of Formaldehyde Vapor by Amine-Functionalized Mesoporous Silica Materials. *J. Environ. Sci.* **2008**, *20* (3), 379.

(16) Ewlad-Ahmed, A. M.; Morris, M. A.; Patwardhan, S. V.; Gibson, L. T. Removal of Formaldehyde from Air Using Functionalized Silica Supports. *Environ. Sci. Technol.* **2012**, *46* (24), 13354.

(17) Wang, Z.; Wang, W.; Jiang, D.; Zhang, L.; Zheng, Y. Diamine-Appended Metal−organic Frameworks: Enhanced Formaldehyde-Vapor Adsorption Capacity, Superior Recyclability and Water Resistibility. *Dalt. Trans.* **2016**, *45* (28), 11306.

(18) Chen, D.; Qu, Z.; Sun, Y.; Wang, Y. Adsorption-Desorption Behavior of Gaseous Formaldehyde on Different Porous Al_2O_3 Materials. *Colloids Surf., A* **2014**, *441*, 433.

(19) Wang, J.; Zhang, P.; Li, J.; Jiang, C.; Yunus, R.; Kim, J. Room-Temperature Oxidation of Formaldehyde by Layered Manganese Oxide: Effect of Water. *Environ. Sci. Technol.* **2015**, *49* (20), 12372.

(20) Ye, J.; Zhu, X.; Cheng, B.; Yu, J.; Jiang, C. Few-Layered Graphene-like Boron Nitride: A Highly Efficient Adsorbent for Indoor Formaldehyde Removal. *Environ. Sci. Technol. Lett.* **2017**, *4* (1), 20.

(21) Chen, X.; Xu, L.; Liu, L. L.; Zhao, L. S.; Chen, C. P.; Zhang, Y.; Wang, X. C. Adsorption of Formaldehyde Molecule on the Pristine and Transition Metal Doped Graphene: First-Principles Study. *Appl. Surf. Sci.* **2017**, *396*, 1020.

(22) Xu, Z.; Yu, J.; Liu, G.; Cheng, B.; Zhou, P.; Li, X. Microemulsion-Assisted Synthesis of Hierarchical Porous $Ni(OH)_2$/SiO_2 Composites toward Efficient Removal of Formaldehyde in Air. *Dalt. Trans.* **2013**, *42* (28), 10190.

(23) Yu, B.; Li, N.; He, W.; Ji, J.; Zhang, S.; Chen, H. Multifunctional Solar Wall for Dehumidification, Heating and Removal of Formaldehyde: Part 1. System Description, Preparation and Performance of SiO_2/TiO_2 Adsorbent. *Build. Environ.* **2016**, *100*, 203.
(24) Eriksson, B.; Johanssin, L.; Svedung, I. "The Nordest Symposium on Air Pollution Abatement by Filtration and Respiratory Protection," 1980.
(25) Sekine, Y.; Nishimura, A. Removal of Formaldehyde from Indoor Air by Passive Type Air-Cleaning Materials. *Atmos. Environ.* **2001**, *35* (11), 2001.
(26) Nomura, A.; Jones, C. W. Amine-Functionalized Porous Silicas as Adsorbents for Aldehyde Abatement. *ACS Appl. Mater. Interfaces* **2013**, *5*, 5569.
(27) Nomura, A.; Jones, C. W. Enhanced Formaldehyde-Vapor Adsorption Capacity of Polymeric Amine-Incorporated Aminosilicas. *Chem. - Eur. J.* **2014**, *20* (21), 6381.
(28) Nomura, A.; Jones, C. W. Airborne Aldehyde Abatement by Latex Coatings Containing Amine-Functionalized Porous Silicas. *Ind. Eng. Chem. Res.* **2015**, *54* (1), 263.
(29) Yu, Y.; Zhang, X.-M.; Ma, J.-P.; Liu, Q.-K.; Wang, P.; Dong, Y.-B. Cu (I)-MOF: Naked-Eye Colorimetric Sensor for Humidity and Formaldehyde in Single-Crystal-to-Single-Crystal Fashion. *Chem. Commun.* **2014**, *50* (12), 1444.
(30) Zou, L.; Luo, Y.; Hooper, M.; Hu, E. Removal of VOCs by Photocatalysis Process Using Adsorption Enhanced TiO_2-SiO_2 Catalyst. *Chem. Eng. Process.* **2006**, *45* (11), 959.
(31) Seo, H. O.; Kim, D. H.; Kim, K.-D.; Park, E. J.; Sim, C. W.; Kim, Y. D. Adsorption and Desorption of Toluene on Nanoporous TiO_2/SiO_2 Prepared by Atomic Layer Deposition (ALD): Influence of TiO_2 Thin Film Thickness and Humidity. *Adsorption* **2013**, *19*, 1181.
(32) Morales-Torres, S.; Carrasco-Marín, F.; Pérez-Cadenas, A.; Maldonado-Hódar, F. Coupling Noble Metals and Carbon Supports in the Development of Combustion Catalysts for the Abatement of BTX Compounds in Air Streams. *Catalysts* **2015**, *5* (2), 774.
(33) Kosuge, K.; Kubo, S.; Kikukawa, N.; Takemori, M. Effect of Pore Structure in Mesoporous Silicas on VOC Dynamic Adsorption/desorption Performance. *Langmuir* **2007**, *23* (6), 3095.
(34) Tidahy, H. L.; Siffert, S.; Lamonier, J. F.; Zhilinskaya, E. a.; Aboukaïs, A.; Yuan, Z. Y.; Vantomme, A.; Su, B. L.; Canet, X.; De Weireld, G.; et al. New Pd/hierarchical Macro-Mesoporous ZrO_2, TiO_2 and ZrO_2-TiO_2 Catalysts for VOCs Total Oxidation. *Appl. Catal., A* **2006**, *310* (1−2), 61.
(35) Wang, H.; Tang, M.; Zhang, K.; Cai, D.; Huang, W.; Chen, R.; Yu, C. Functionalized Hollow Siliceous Spheres for VOCs Removal with High Efficiency and Stability. *J. Hazard. Mater.* **2014**, *268*, 115.
(36) Carlos-Cuellar, S.; Li, P.; Christensen, A. P.; Krueger, B. J.; Burrichter, C.; Grassian, V. H. Heterogeneous Uptake Kinetics of Volatile Organic Compounds on Oxide Surfaces Using a Knudsen Cell Reactor: Adsorption of Acetic Acid, Formaldehyde, and Methanol on α-Fe_2O_3, α-Al_2O_3, and SiO_2. *J. Phys. Chem. A* **2003**, *107* (21), 4250.
(37) Chen, F.; Liu, S.; Yu, J. Efficient Removal of Gaseous Formaldehyde in Air Using Hierarchical Titanate Nanospheres with in Situ Amine Functionalization. *Phys. Chem. Chem. Phys.* **2016**, *18* (27), 18161.
(38) Ortiz De Zarate, D.; Gomez-Moratalla, A.; Guillem, C.; Beltran, A.; Latorre, J.; Beltran, D.; Amoros, P. High-Zirconium-Content Nano-Sized Bimodal Mesoporous Silicas. *Eur. J. Inorg. Chem.* **2006**, *2006* (13), 2572.
(39) Zhao, T.; Jeremias, F.; Boldog, I.; Nguyen, B.; Henninger, S. K.; Janiak, C. High-Yield, Fluoride-Free and Large-Scale Synthesis of MIL-101(Cr). *Dalton Trans.* **2015**, *44* (38), 16791.
(40) Yang, R. T. *Adsorbents: Fundamentals and Applications*; Wiley, 2003.
(41) Fenelonov, V. B.; Romannikov, V. N.; Derevyankin, A. Y. Mesopore Size and Surface Area Calculations for Hexagonal Mesophases (Types MCM-41, FSM-16, Etc.) Using Low-Angle XRD and Adsorption Data. *Microporous Mesoporous Mater.* **1999**, *28* (1), 57.
(42) Pérez-Cabero, M.; Hungría, A. B.; Morales, J. M.; Tortajada, M.; Ramón, D.; Moragues, A.; El Haskouri, J.; Beltrán, A.; Beltrán, D.; Amorós, P. Interconnected Mesopores and High Accessibility in UVM-7-like Silicas. *J. Nanopart. Res.* **2012**, *14* (8), 1045.
(43) Wang, Z.; Wang, W.; Jiang, D.; Zhang, L.; Zheng, Y. Diamine-Appended Metal-Organic Framework: Enhanced Formaldehyde-Vapor Adsorption Capacity, Superior Recyclability and Water Resistibility. *Dalt. Trans.* **2016**, *45* (28), 11306.
(44) Fu, X.; Clark, L. A.; Yang, Q.; Anderson, M. A. Enhanced Photocatalytic Performance of Titania-Based Binary Metal Oxides: TiO_2/SiO_2 and TiO_2/ZrO_2. *Environ. Sci. Technol.* **1996**, *30* (2), 647.
(45) Busca, G.; Lamotte, J.; Lavalley, J. C.; Lorenzelli, V. FT-IR Study of the Adsorption and Transformation of Formaldehyde on Oxide Surfaces. *J. Am. Chem. Soc.* **1987**, *109* (17), 5197.
(46) Shibata, K.; Kiyoura, T.; Kitagawa, J.; Sumiyoshi, T.; Tanabe, K. Acidic Properties of Binary Metal Oxides. *Bull. Chem. Soc. Jpn.* **1973**, *46*, 2985−2988.
(47) Zecchina, a.; Bordiga, S.; Lamberti, C.; Ricchiardi, G.; Lamberti, C.; Ricchiardi, G.; Scarano, D.; Petrini, G.; Leofanti, G.; Mantegazza, M. Structural Characterization of Ti Centres in Ti-Silicalite and Reaction Mechanisms in Cyclohexanone Ammoximation. *Catal. Today* **1996**, *32* (1−4), 97.
(48) Neumayer, D. A.; Cartier, E. Materials Characterization of ZrO_2−SiO_2 and HfO_2−SiO_2 Binary Oxides Deposited by Chemical Solution Deposition. *J. Appl. Phys.* **2001**, *90* (4), 1801.
(49) Zeitler, V. A.; Brown, C. A. The Infrared Spectra of Some Ti-O-Si, Ti-O-Ti and Si-O-Si Compounds. *J. Phys. Chem.* **1957**, *61* (9), 1174.
(50) Adamczyk, A.; Długoń, E. The FTIR Studies of Gels and Thin Films of Al_2O_3-TiO_2 and Al_2O_3-TiO_2-SiO_2 Systems. *Spectrochim. Acta, Part A* **2012**, *89*, 11.
(51) Yu, J.; Zhao, X.; Yu, J.; Zhong, G.; Han, J.; Zhao, Q. The Grain Size and Surface Hydroxyl Content of Super-Hydrophilic TiO_2/SiO_2 Composite Nanomeer Thin Films. *J. Mater. Sci. Lett.* **2001**, *20*, 1745.
(52) Lucovsky, G.; Rayner, G. B. Microscopic Model for Enhanced Dielectric Constants in Low Concentration SiO_2-Rich Noncrystalline Zr and Hf Silicate Alloys. *Appl. Phys. Lett.* **2000**, *77* (18), 2912.

DOI: 10.1021/acs.iecr.8b02962
Ind. Eng. Chem. Res. 2018, 57, 12916−12925